Published in final edited form as:
Cereb Cortex. 2003 July ; 13(7): 722–727.

Distribution of Non-phosphorylated Neurofilament in Squirrel Monkey V1 Is Complementary to the Pattern of Cytochrome-oxidase Blobs

Kevin R. Duffy and **Margaret S. Livingstone**
Department of Neurobiology, Harvard Medical School, 220 Longwood Ave, Boston, MA 02115, USA

Abstract

The geniculo-recipient zones of the primate primary visual cortex (V1) stain more strongly for cytochrome oxidase (CO) than other regions. Labeling V1 with an antibody (SMI-32) against neurofilament protein produces a laminar pattern that is largely complementary to that of CO: the layers that receive the strongest geniculate input react weakly for SMI-32. We evaluated whether the complementary laminar relationship extends throughout the superficial layers where there are regularly spaced blobs of dark CO staining that are known to receive geniculate input. In all hemispheres, neurofilament labeling in the superficial layers was indeed complementary to the CO pattern. The density of SMI-32 labeled neurons was quantified and found to be greater within the CO interblobs than in the blobs. These results demonstrate that blobs and interblobs can be distinguished by examining the pattern of neurofilament expression in V1. That neurofilament expression is highest within interblobs raises the possibility that the distribution of cell types may be non-uniform across blobs and interblobs.

Introduction

Within the primary visual cortex (V1) there is a set of organized columns that process a variety of features such as orientation, color and ocular dominance (Hubel and Wiesel, 1968; Livingstone and Hubel, 1984). One of the most commonly studied columnar organizations in V1 is the cytochrome oxidase (CO) blobs (Horton and Hubel, 1981; Carroll and Wong-Riley, 1984; Horton, 1984; Livingstone and Hubel, 1984; Murphy *et al*., 1995). Sections of primate V1 cut tangential to the cortical surface and reacted for the mitochondrial enzyme CO show regularly spaced blobs of staining. Although these blobs are most obvious in the superficial layers, they can also be seen, albeit faintly, in layers IVB, V and VI (Carroll and Wong-Riley, 1984; Horton, 1984). The CO-rich neurons that comprise blobs are believed to be more physiologically active than neurons located within interblobs (Livingstone and Hubel, 1984), and this is supported by the finding that 2-deoxyglucose uptake in V1 aligns with CO blobs (Horton and Hubel, 1981; Humphrey and Hendrickson, 1983).

Blobs can be distinguished from interblobs using many stains and labels besides CO. Blobs can be identified using glutamic acid decarboxylase (Hendrickson *et al*., 1981), lactate dehydrogenase, succinate dehydrogenase, acetylcholinesterase (Horton, 1984), CAT301 (Hendry *et al*., 1984), NADPH diaphorase (Sandell, 1986), microtubule-associated protein 2 (Hendry and Bhandari, 1992), parvalbumin (Johnson and Casagrande, 1995), and AMPA receptor subunits (Carder, 1997). Interestingly, there are fewer markers that are known to

Address correspondence to Kevin Duffy, Department of Neurobiology, Harvard Medical School, 220 Longwood Ave., Boston, MA 02115, USA. Email: kevin_duffy@hms.harvard.edu..

preferentially identify interblobs. These markers include calbindin (Celio *et al.*, 1986; Hendry and Carder, 1993; Blumcke *et al*., 1994; Johnson and Casagrande, 1995), calcineurin (Goto and Singer, 1994), zinc (Dyck and Cynader, 1993), and the muscarinic cholinergic receptor protein m2 (Tigges *et al*., 1997). Although it is not known how these differences relate to the ability of the visual cortex to process stimulus features, a thorough understanding of blob and interblob anatomy may offer some insight.

In primate V1, the layers that receive the strongest geniculate input [IVA, IVCα and IVCβ (Hubel and Wiesel, 1972; Hendrickson *et al*., 1978)] have the highest levels of CO (Horton, 1984; Livingstone and Hubel, 1984). The same relationship is found throughout the superficial layers where the geniculate input zones are non-uniformly distributed and overlap with the CO-rich blobs (Livingstone and Hubel, 1982; Lachica and Casagrande, 1992). In contrast, the laminar pattern of non-phosphorylated neurofilament (labeled with the antibody SMI-32) is complementary to that of CO: layers IVA, IVCα and IVCβ have the lowest levels of SMI-32 (Hof and Morrison, 1995; Chaudhuri *et al*., 1996). In the present experiment we wanted to evaluate whether the complementary relationship between CO and SMI-32 extends tangentially throughout the superficial layers where the patterns of CO and geniculate inputs are non-uniform. To test this, we compared the expression pattern of SMI-32 labeled cells to the pattern of CO staining within the superficial layers.

Materials and Methods

Animals

The patterns of CO and SMI-32 were examined in six hemispheres from four normal adult squirrel monkeys. All procedures were approved by the Harvard Medical Area Standing Committee on Animals.

Histology

Animals were killed with a lethal dose of Nembutal (50 mg/kg) and perfused transcardially with cold 0.9% saline (4°C, 200-250 ml) until the circulating fluid was clear, followed by cold (4°C) 4% paraformaldehyde in phosphate-buffered saline, pH 7.4 (200-300 ml). The brain was then removed from the skull, and V1 from each hemisphere was gently flattened between glass slides and postfixed in 4% paraformaldehyde with 30% sucrose for 30 min. The flattened cortex was then transferred to phosphate-buffered saline with 30% sucrose and allowed to free float overnight. The tissue was cut tangentially into 50 μm sections using a freezing microtome. All hemispheres followed this procedure with the exception of one that was cut in the coronal plane.

Adjacent sections were reacted for CO or non-phosphorylated neurofilament protein using the antibody SMI-32 (Sternberger Monoclonals, Lutherville, MD), so that a direct comparison between the two labeling patterns could be achieved. SMI-32 is a monoclonal antibody that recognizes a non-phosphorylated epitope on heavy and medium molecular weight subunits of neurofilament protein (Lee *et al*., 1988). Free floating tissue sections cut for SMI-32 immunoreactivity were first placed in cold methanol with 0.3% hydrogen peroxide for 5 min and then pre-incubated for 1 h in Tris-buffered saline (TBS) containing 0.1% Triton X-100 and 5% normal goat serum. Sections were then incubated overnight in TBS containing 0.1% Triton X-100, 5% normal goat serum, and primary monoclonal antibody against non-phosphorylated neurofilament protein (1:2000). On the following day, immunoreactivity was revealed using a Vectastain ABC kit (Vector Laboratories, Burlingame, CA) and chromogen 3,3′-diaminobensidine (DAB) with peroxide.

CO staining followed procedures outlined previously (Wong-Riley, 1979; Horton, 1984; Murphy *et al*., 1995). Sections cut for CO reactivity were mounted on gelatin-coated glass slides and air dried overnight. The next day, sections were incubated in phosphate buffer (0.1 M, pH 7.4) that contained a mixture of cytochrome C oxidase, catalase and DAB. Sections were reacted at 40°C in an incubator until the maximal contrast between blobs and interblobs was obtained (~8 h). Sections were then dehydrated in a series of graded alcohols, defatted in xylenes, and then coverslipped with DPX (BDH Labs, Poole, UK).

Quantification

A comparison of tangential sections labeled for neurofilament and CO was achieved by aligning adjacent sections using the radial blood vessel pattern. The boundaries around CO blobs were determined in an automated fashion using a Matlab routine that identified blob borders by drawing a contour at half the maximum to minimum optical staining intensity within the analysis area. Quantification of cell density in blobs and interblobs was performed for each tangentially cut hemisphere ($n = 5$) and involved using a computer application (Neurolucida, MicroBrightField, Inc., Williston, UT) to plot individually labeled neurons under high magnification. Cell plots from each animal were taken from the same retinotopic region of V1 (parafoveal) and represented an area of cortex that was ~5 mm^2. The cell plots were spatially aligned with the blob contour map using the pattern of radial blood vessels, and a calculation of cell density (neurons/mm^2) inside and outside of blobs was made. Cells that were not clearly within a blob or interblob (~10% of our sample) were not included in the analysis. Using a binomial distribution analysis, we also calculated the probability that the observed distribution of SMI-32 labeled cells relative to CO blobs occurred by chance.

Results

A distinct laminar pattern was found when coronal sections of squirrel monkey V1 were reacted for SMI-32 (Fig. 1). These results are consistent with those of others (Hof and Morrison, 1995;Chaudhuri *et al*., 1996), namely, that SMI-32 positive cells were found primarily in layers II/III, IVB, V and VI. Labeled neurons were most often pyramidal in shape and frequently the dendritic fields of these cells were visible. The layers of V1 that receive the heaviest geniculate input, and are highly reactive for CO (IVA, IVCα and IVCβ), were weakly labeled for SMI-32.

In flattened sections cut tangential to the cortical surface, the superficial layers of squirrel monkey V1 showed a non-uniform distribution of SMI-32 labeling (Fig. 2*B*). Darkly labeled neurons clustered around regularly spaced patches of reduced labeling, giving rise to a honeycomb pattern. Qualitatively, the pattern of SMI-32 poor patches was similar to that of CO blobs. We compared the spatial relationship between these two features by aligning adjacent sections reacted for either CO (Fig. 2*A*) or SMI-32 (Fig. 2*B*). Borders around blobs were calculated automatically and compared with the pattern of SMI-32 (Fig. 2*C,D*). The two patterns were complementary: CO blobs aligned with the lightly labeled patches of SMI-32, meaning that most SMI-32 positive neurons were found within interblobs. To further examine this relationship we plotted the distribution of individual SMI-32 positive neurons and compared it to the pattern of CO blobs (Fig. 2*E,F*). This analysis confirmed that the majority of SMI-32 positive cells were located within inter-blobs.

At higher magnification, the pattern of SMI-32 can be seen to result from labeled cell bodies and their dendrites (Fig. 3*A,C*), as well as the shafts of apical dendrites extending from neurons positioned deeper in the cortex (arrows in Fig. 3*C*). SMI-32 positive cell bodies tended to congregate outside of blobs; however, the basal dendrites from some of these cells were seen to cross into blob territory.

Figure 4 shows another example of the relationship between CO staining and SMI-32 labeling in V1 from a different monkey. As with the previous example, the majority of SMI-32 labeled neurons in the superficial layers were located within CO interblobs (Fig. 4*E*,*F*). This example also illustrates the point that not all SMI-32 positive neurons are found within interblobs. In some cases, labeled neurons were clearly located within a CO blob. Therefore, these findings demonstrate a tendency rather than an absolute rule for SMI-32 labeling to be located outside of CO blobs. This same pattern of results was found in three additional hemispheres (not shown).

Examination of consecutive sections through the superficial layers (Fig. 5) revealed that the pattern of SMI-32 labeling was present first in layer I (Fig. 5*A*). At high magnification it was clear that the labeling in layer I was largely due to apical dendrite shafts that extended from cells located in deeper layers. The pattern of SMI-32 labeled somata became obvious as soon as the pattern of CO blobs emerged (Fig. 5*B*). The SMI-32 pattern was found throughout layers II/III but was most obvious near the middle of these layers, where the blob pattern was clearest; ~200-300 μm below the cortical surface (Fig. 5*C*). Throughout the superficial layers, SMI-32 labeling was heaviest outside of CO blobs and consistently resembled a honeycomb. As the pattern of CO blobs faded, so too did the pattern of SMI-32 labeling.

To quantify these results, a calculation of neuronal density was made for SMI-32 labeling inside and outside of CO blobs (see methods). Approximately 10% of immunoreactive cells were within 25 μm of a blob/interblob border and were not clearly inside or outside of a blob. Therefore, these border cells were not included in our density analysis. A total of 2047 cells from five hemispheres were included in our sample, 1721 (~84%) of these were clearly located within interblobs, and 132 (~6%) were found within blobs. Because blobs take up less area than interblobs (~30% of the total area), we calculated the density of cells per area of cortex within both regions. Our density analysis (Fig. 6) revealed that there were significantly more SMI-32 positive neurons located within CO interblobs compared to blobs (*t*-test, $P < 0.001$). The average density inside a blob was 27 neurons/mm^2 (SEM = 3.6) while the average density within an interblob was 116 neurons/mm^2 (SEM = 12.1). Using a binomial distribution analysis, we also calculated the probability that the observed distribution of SMI-32 labeled cells relative to blobs could have occurred by chance. For each of the hemispheres we examined, the probability that these results occurred by chance was <0.0001.

Discussion

We examined the distribution of SMI-32 labeling in the superficial layers from tangentially cut sections of V1 and compared this to the pattern of CO blobs. SMI-32 positive neurons were more frequently located within interblobs and less often within blobs.

We are confident that our observed SMI-32 immunoreactivity is specific for the targeted antigen for the following reasons. (i) The pattern of reactivity for SMI-32 that we observed in coronal sections is consistent with previous findings that used the same antibody (Hof and Morrison, 1995; Chaudhuri *et al*., 1996; Kogan *et al*., 2000; Fenstemaker *et al*., 2001). (ii) In agreement with past reports (Sternberger and Sternberger, 1983; Hof and Morrison, 1995), our labeling was primarily observed within the perikarya and dendrites of large pyramidal cells. (iii) Control sections that were reacted in the absence of primary antibody were devoid of label.

The pattern of SMI-32 labeling observed here may be related to the distribution of calcineurin labeling in the superficial layers of V1. Calcineurin is a calcium/calmodulin-dependent protein phosphatase that influences the phosphorylation state of cytoskeleton proteins (Goto *et al*., 1985). In coronal sections of V1, calcineurin and SMI-32 have similar laminar labeling patterns, and both primarily target pyramidal neurons (Goto and Singer, 1994; Hof and

Morrision, 1995). Our results reveal another similarity, namely that, like calcineurin (Goto and Singer, 1994), SMI-32 expression is heaviest within CO interblobs. That these two anatomical features overlap in the visual cortex is in agreement with the role that calcineurin has in the dephosphorylation of cytoskeleton proteins (Goto *et al*., 1985). Our finding of an accumulation of non-phosphorylated neurofilament protein (labeled by SMI-32) within interblobs helps to explain the overlapping patterns of calcineurin and SMI-32 expression.

The SMI-32 antibody labels large pyramidal neurons (Meynert cells) within the infragrangular layers of V1 (see Fig. 1). It has previously been shown that Meynert cells are non-uniformly distributed across the infragranular layers such that they are largely located outside of CO blobs (Fries, 1986;Payne and Peters, 1989). Only 3% of Meynert cells fall within blob regions, with the remaining cells located either along blob borders or within interblobs (Fries, 1986). Our results demonstrate the same pattern in the superficial layers, with the majority of supragranular SMI-32 positive cells being located outside of blob centers.

A non-uniform distribution of SMI-32 labeling has been observed in the superficial layers of macaque monkey V1; however, this pattern was not reported to have a consistent spatial relationship to CO blobs (Fenstemaker *et al*., 2001). The observed lack of correlation between these two markers in the macaque may be the consequence of a less distinct blob pattern. In squirrel monkey V1, the pattern of CO blobs is clearer, more punctate, and better demarcated compared to macaque blobs (Horton, 1984). This may make it difficult to determine a spatial relationship between SMI-32 and CO in macaque without a quantitative analysis.

Neurons reactive for SMI-32 are mostly large in size and pyramidal in shape. This raises the possibility that the pattern of SMI-32 expression in the superficial layers is due to a non-uniform distribution of pyramidal neurons. Although pyramidal cells inside and outside of CO blobs do not differ in their soma size, spine density, or basal dendritic field structure (Hubener and Bolz, 1992), the distribution of pyramidal cells with respect to the CO pattern has not been studied quantitatively. A non-uniform distribution of pyramidal cells in the superficial layers of V1 could explain the inhomogeneous SMI-32 expression. If pyramidal cells were unevenly distributed so that the geniculate recipient zones (blobs) contained fewer of them, SMI-32 expression would be expected to be greatest outside of blobs.

Similar to primate V1, the rat primary somatosensory cortex (SI) has a distinct anatomical and physiological compartmentalization. Within SI there are patches of neurons—called barrels—that stain darkly for CO (Land and Simons, 1985) and each receives a projection, via the thalamus, from only one vibrissa (Woolsey and Van der Loos, 1970). The regions of cortex that separate barrels, known as septa, exhibit weaker staining for CO (Land and Simons, 1985) and thus give rise to a pattern of dark patches known as barrel fields. Interestingly, SMI-32 labeling is heaviest outside the CO-rich barrels and exhibits greatest expression within septa (Pegado *et al*., 1996). These results are similar to our findings and support the notion that SMI-32 labeling is complementary to the pattern of CO and thalamic inputs.

In V1, SMI-32 labeling is weak in the regions of layer IV (IVA, IVCα and IVCβ) and layers II/II (blobs) that receive geniculate input, however, not all geniculo-recipient layers show weak expression. Layer VI receives a sparse geniculate input (Hubel and Wiesel, 1972; Lund, 1988) and exhibits heavy SMI-32 labeling. Therefore, not all layers that receive geniculate input express weak SMI-32. Perhaps the arrangement and degree of geniculate input influences the patterns of CO and SMI-32 in complementary ways. This issue could be addressed with a comprehensive analysis of the relationship between the pattern of geniculate input and the expression of CO and SMI-32 in layer VI.

The growing number of reports that document anatomical differences between blobs and interblobs indicate that these are features of V1 that can be distinguished by more than simply

the level of CO. The anatomical features that make blobs and interblobs unique are likely the same features that endow them with the ability to perform different physiological functions. Although blob and interblob neurons have distinct physiological properties (Livingstone and Hubel, 1984; Landisman and Ts'o, 2002), little is known about how their anatomical features are related to their unique functions. A better understanding of the anatomical differences between blobs and interblobs could provide valuable information toward understanding their role in the visual system.

Acknowledgements

This work was supported by NEI grant EY13135 to M.S.L., postdoctoral fellowships from Fight for Sight and NSERC to K.R.D., and NEI grant EY12196 (Core Grant for Vision Research). The authors thank Vladimir Berezovskii, Christopher Pack and Bevil Conway for helpful comments on the manuscript.

References

Blumcke I, Weruaga E, Kasas S, Hendrickson AE, Celio MR. Discrete reduction patterns of parvalbumin and calbindin D-28k immunoreactivity in the dorsal lateral geniculate nucleus and the striate cortex of adult macaque monkeys after monocular enucleation. Vis Neurosci 1994;11:1–11. [PubMed: 8011573]

Carder RK. Immunocytochemical characterization of AMPA-selective glutamate receptor subunits: laminar and compartmental distribution in macaque striate cortex. J Neurosci 1997;17:3352–3363. [PubMed: 9096168]

Carroll EW, Wong-Riley MT. Quantitative light and electron microscopic analysis of cytochrome oxidase-rich zones in the striate cortex of the squirrel monkey. J Comp Neurol 1984;222:1–17. [PubMed: 6321561]

Celio MR, Scharer L, Morrison JH, Norman AW, Bloom FE. Calbindin immunoreactivity alternates with cytochrome c-oxidase-rich zones in some layers of the primate visual cortex. Nature 1986;323:715–717. [PubMed: 3022149]

Chaudhuri A, Zangenehpour S, Matsubara JA, Cynader MS. Differential expression of neurofilament protein in the visual system of the vervet monkey. Brain Res 1996;709:17–26. [PubMed: 8869552]

Dyck RH, Cynader MS. An interdigitated columnar mosaic of cytochrome oxidase, zinc, and neurotransmitter-related molecules in cat and monkey visual cortex. Proc Natl Acad Sci USA 1993;90:9066–9069. [PubMed: 8415654]

Fenstemaker SB, Kiorpes L, Movshon JA. Effects of experimental strabismus on the architecture of macaque monkey striate cortex. J Comp Neurol 2001;438:300–317. [PubMed: 11550174]

Fries W. Distribution of Meynert cells in primate striate cortex. Spatial relationships with cytochrome oxidase blobs. Naturwissenschaften 1986;73:557–558. [PubMed: 3020436]

Goto S, Singer W. Laminar and columnar organization of immunoreactivity for calcineurin, a calcium- and calmodulin-regulated protein phosphatase, in monkey striate cortex. Cereb Cortex 1994;4:636–645. [PubMed: 7703689]

Goto S, Yamamoto H, Fukunaga K, Iwasa T, Matsukado Y, Miyamoto E. Dephosphorylation of microtubule-associated protein 2, τ factor, and tubulin by calcineurin. J Neurochem 1985;45:276–283. [PubMed: 2987415]

Hendrickson AE, Wilson JR, Ogren MP. The neuroanatomical organization of pathways between the dorsal lateral geniculate nucleus and visual cortex in Old World and New World primates. J Comp Neurol 1978;182:123–136. [PubMed: 100530]

Hendrickson AE, Hunt SP, Wu JY. Immunocytochemical localization of glutamic acid decarboxylase in monkey striate cortex. Nature 1981;292:605–607. [PubMed: 6265804]

Hendry SH, Hockfield S, Jones EG, McKay R. Monoclonal antibody that identifies subsets of neurones in the central visual system of monkey and cat. Nature 1984;307:267–269. [PubMed: 6694727]

Hendry SH, Bhandari MA. Neuronal organization and plasticity in adult monkey visual cortex: immunoreactivity for microtubule-associated protein 2. Vis Neurosci 1992;9:445–459. [PubMed: 1333277]

Hendry SH, Carder RK. Neurochemical compartmentation of monkey and human visual cortex: similarities and variations in calbindin immunoreactivity across species. Vis Neurosci 1993;10:1109–1120. [PubMed: 8257667]

Hof PR, Morrison JH. Neurofilament protein defines regional patterns of cortical organization in the macaque monkey visual system: a quantitative immunohistochemical analysis. J Comp Neurol 1995;352:161–186. [PubMed: 7721988]

Horton JC. Cytochrome oxidase patches: a new cytoarchitectonic feature of monkey visual cortex. Phil Trans R Soc Lond B Biol Sci 1984;304:199–253. [PubMed: 6142484]

Horton JC, Hubel DH. Regular distribution of cytochrome oxidase staining in primary visual cortex of macaque monkey. Nature 1981;292:762–764. [PubMed: 6267472]

Hubel DH, Wiesel TN. Receptive fields and functional architecture of monkey striate cortex. J Physiol 1968;195:215–243. [PubMed: 4966457]

Hubel DH, Wiesel TN. Laminar and columnar distribution of geniculo-cortical fibers in the macaque monkey. J Comp Neurol 1972;146:421–450. [PubMed: 4117368]

Hubener M, Bolz J. Relationships between dendritic morphology and cytochrome oxidase compartments in monkey striate cortex. J Comp Neurol 1992;324:67–80. [PubMed: 1328331]

Humphrey AL, Hendrickson AE. Background and stimulus-induced patterns of high metabolic activity in the visual cortex (area 17) of the squirrel and macaque monkey. J Neurosci 1983;3:345–358. [PubMed: 6296333]

Johnson JK, Casagrande VA. Distribution of calcium-binding proteins within the parallel visual pathways of a primate (*Galago crassicaudatus*). J Comp Neurol 1995;356:238–260. [PubMed: 7629317]

Kogan CS, Zangenehpour S, Chaudhuri A. Developmental profiles of SMI-32 immunoreactivity in monkey striate cortex. Brain Res Dev Brain Res 2000;119:85–95.

Lachica EA, Casagrande VA. Direct W-like geniculate projections to the cytochrome oxidase (CO) blobs in primate visual cortex: axon morphology. J Comp Neurol 1992;319:141–158. [PubMed: 1375606]

Land PW, Simons DJ. Cytochrome oxidase staining in the rat smI barrel cortex. J Comp Neurol 1985;238:225–235. [PubMed: 2413086]

Landisman CE, Ts'o DY. Color processing in macaque striate cortex: electrophysiological properties. J Neurophysiol 2002;87:3138–3151. [PubMed: 12037214]

Lee VM, Otvos YL, Carden MJ, Hollosi M, Dietzschold B, Lazzarini RA. Identification of the major multiphosphorylation site in mammalian neurofilaments. Proc Natl Acad Sci USA 1988;85:1998–2002. [PubMed: 2450354]

Livingstone MS, Hubel DH. Thalamic inputs to cytochrome oxidase-rich regions in monkey visual cortex. Proc Natl Acad Sci USA 1982;79:6098–6101. [PubMed: 6193514]

Livingstone MS, Hubel DH. Anatomy and physiology of a color system in the primate visual cortex. J Neurosci 1984;4:309–356. [PubMed: 6198495]

Lund JS. Anatomical organization of macaque monkey striate visual cortex. Ann Rev Neurosci 1988;11:253–288. [PubMed: 3284442]

Murphy KM, Jones DG, Van Sluyters RC. Cytochrome-oxidase blobs in cat primary visual cortex. J Neurosci 1995;15:4196–4208. [PubMed: 7790905]

Payne BR, Peters A. Cytochrome oxidase patches and Meynert cells in monkey visual cortex. Neuroscience 1989;28:353–363. [PubMed: 2537938]

Pegado V, Froc D, Spironello E, Murphy KM. Rat somatosensory cortex: an anatomical substrate for bilateral integration. Soc Neurosci Abstr 1996;22:105.

Sternberger LA, Sternberger NH. Monoclonal antibodies distinguish phosphorylated and non-phosphorylated forms of neurofilament *in situ*. Proc Natl Acad Sci USA 1983;80:6126–6130. [PubMed: 6577472]

Sandell JH. NADPH diaphorase histochemistry in the macaque striate cortex. J Comp Neurol 1986;251:388–397. [PubMed: 3771835]

Tigges M, Tigges J, Rees H, Rye D, Levey AI. Distribution of muscarinic cholinergic receptor proteins m1 to m4 in area 17 of normal and monocularly deprived rhesus monkeys. J Comp Neurol 1997;388:130–145. [PubMed: 9364243]

Wong-Riley MTT. Changes in the visual system of monocularly sutured or enucleated cat demonstrable with cytochrome oxidase histochemistry. Brain Res 1979;171:11–28. [PubMed: 223730]

Woolsey TA, Van der Loos H. The structural organization of layer IV in the somatosensory region (SI) of mouse cerebral cortex. Brain Res 1970;17:205–232. [PubMed: 4904874]

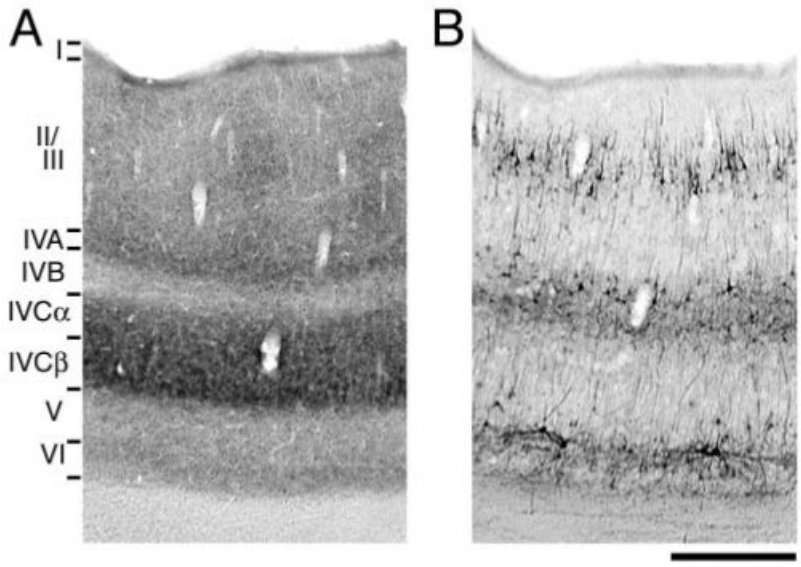

Figure 1.
Adjacent coronal sections of squirrel monkey V1 labeled for CO (*A*) and SMI-32 (*B*). As demonstrated in previous studies, the layers richest in CO (IVA, IVCα and IVCβ) were weakly labeled for SMI-32. Scale bar = 500 μm.

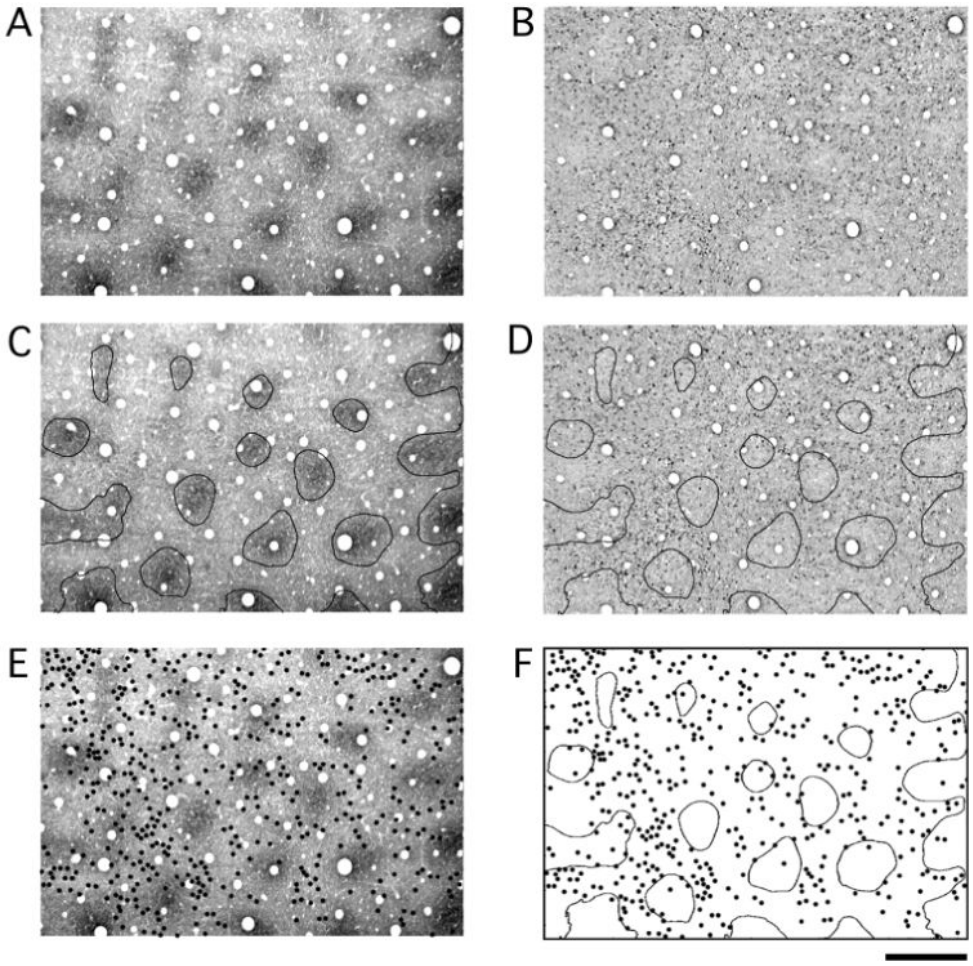

Figure 2.

Tangentially cut sections of V1 labeled for CO (*A*) and SMI-32 (*B*). Adjacent sections were aligned using the pattern of radial blood vessels. CO blobs were identified in an automated way and contours were drawn around the border of each blob (*C*). The blob contours were then superimposed onto the section labeled for SMI-32. The heaviest SMI-32 labeling was found outside blob centers (*D*). Each SMI-32 positive cell was identified under a microscope and a dot was placed at its location in the adjacent CO section (*E*). The distribution of blob contours and SMI-32 positive cells was then examined (*F*). This analysis revealed a tendency for SMI-32 positive neurons to be located within interblobs. Scale bar = 500 μm.

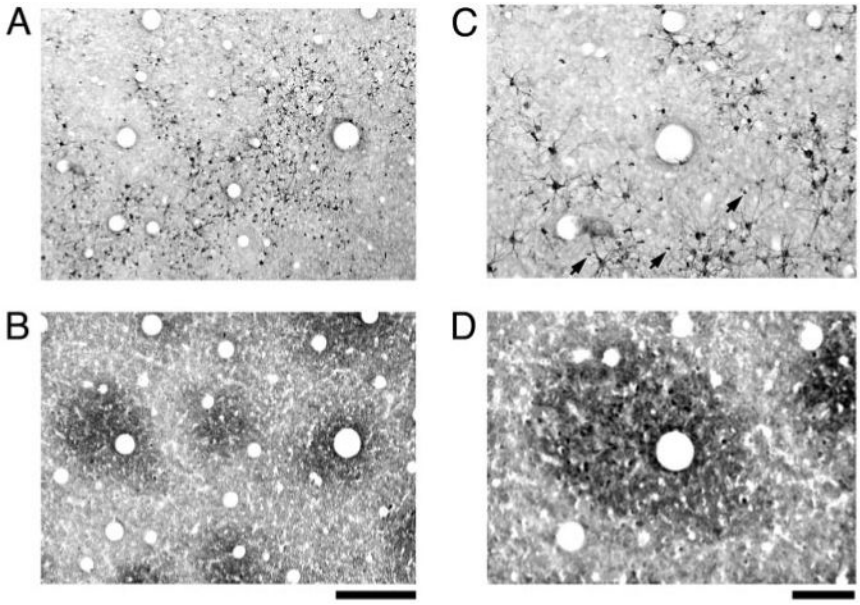

Figure 3.
High magnification photographs of SMI-32 immunoreactivity (*A* and *C*) and CO staining (*B* and *D*). The pattern of SMI-32 was comprised of dark neuronal somata and dendritic processes, as well as apical dendrites from deeper neurons that created a punctate pattern outside of blobs (arrows in *B*). At this magnification, individual SMI-32 positive cells could be seen to lie primarily outside of blobs. Scale bars = 250 μm (*A* and *B*) and 100 μm (*C* and *D*).

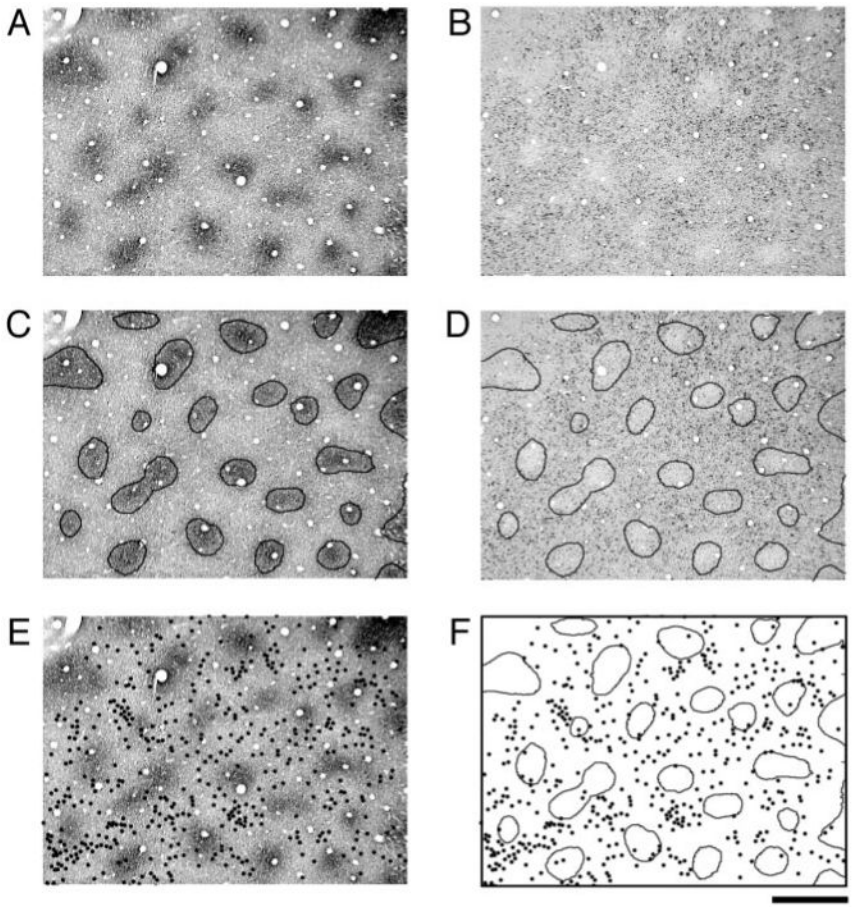

Figure 4.

Another example of the relationship between CO blobs (*A*) and SMI-32 labeling (*B*) in V1 from a different monkey. The regions defined by contours generated around CO blobs (*C*) were within regions that were light for SMI-32 labeling (*D*). Individual SMI-32 positive neurons were plotted as black dots superimposed onto the adjacent CO section (*E*). Comparison of these two patterns shows that SMI-32 labeled cells fall preferentially within inter-blob regions (*F*). Scale bar = 500 μm.

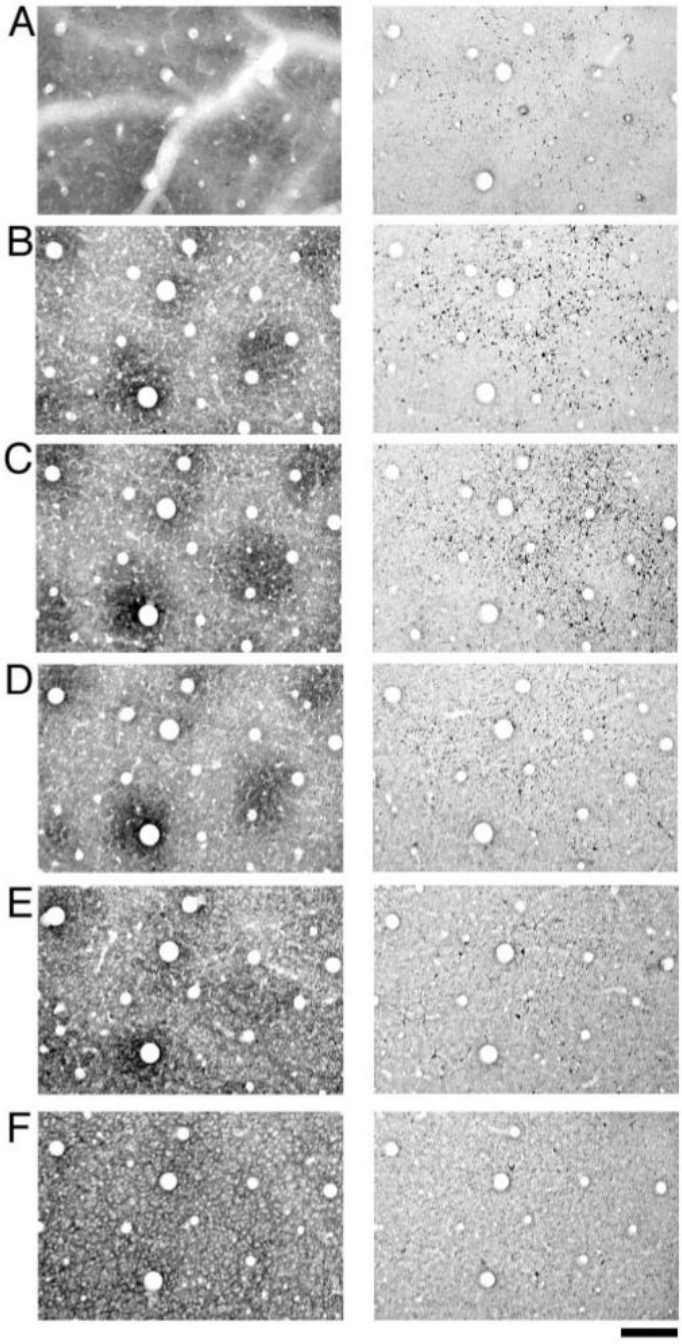

Figure 5.
A sequential series of sections reacted for CO (left column) or SMI-32 (right column). The sections start at the top of layer I (row *A*), move through layers II/III (rows *B, C* and *D*) and end in layer IVA (row *F*). SMI-32 labeling was apparent in the most superficial sections examined and consisted of apical dendrite shafts (row A). Sections taken from layers II/III (rows *B, C* and *D*) revealed a distribution of SMI-32 labeled cells that clustered outside of CO blobs. Sections sampled from deep layer III and layer IVA show weak SMI-32 labeling with the distribution of cells not showing a strong correlation with the CO pattern (*E* and *F*). Scale bar = 200 μm.

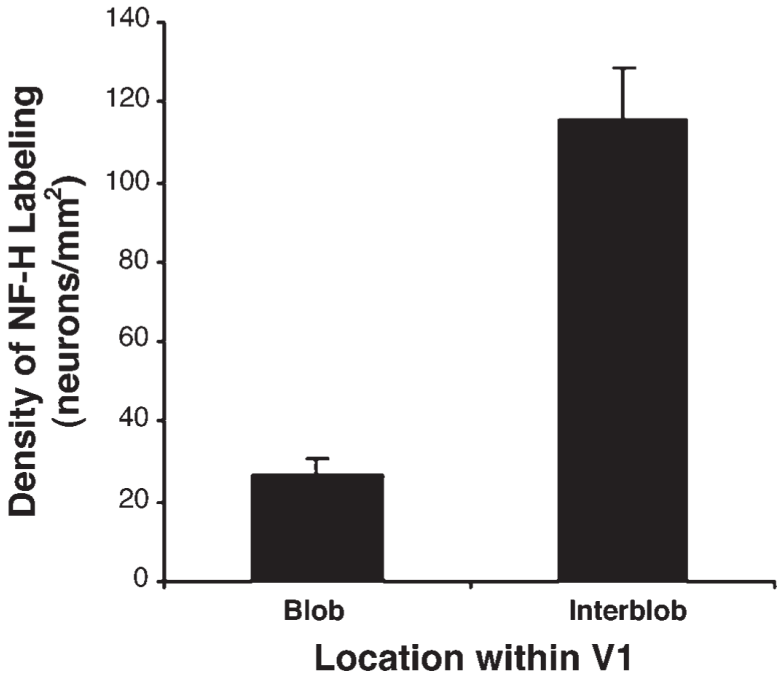

Figure 6.
Quantification of the spatial relationship between SMI-32 labeling and CO blobs. The distribution of SMI-32 labeled cells was plotted from a 5 mm^2 area of V1 for each of the five hemispheres we examined. In this graph, the density of labeled cells inside of blobs and interblobs is plotted. The density of SMI-32 positive neurons is significantly greater within interblobs ($P < 0.001$; *t*-test). Error bars represent the standard error of the mean.